Photophysical and Electrochemical Properties of Blue Phosphorescent Iridium(III) Complexes

Li-Lan Wu,[†] Cheng-Hsien Yang,*[,‡] I-Wen Sun,*[,†] Sheng-Yuan Chu,[§] Po-Ching Kao,[§] and Hsin-Hsuan Huang[§]

Department of Chemistry, National Cheng Kung University, Tainan, Taiwan, 701, Republic of China, Carbon Nanocapsules Research Department, Nano-Powder & Thin Film Technology Center, ITRI South, Tainan, Taiwan, 709, Republic of China, and Department of Electrical Engineering, National Cheng Kung University, Tainan, Taiwan, 701, Republic of China

Received December 3, 2006

A series of 2-difluorophenyl-4-methoxypyridine ligands were synthesized and successfully used to prepare iridium complexes including bis[2-(2′,3′-difluorophenyl)-4-methoxypyridinato-*N*,$C^{2'}$]iridium(III) [5-(2′-pyridyl)tetrazolate] (**5a1**), bis[2-(2′,4′-difluorophenyl)-4-methoxypyridinato-*N*,$C^{2'}$]iridium(III) [5-(2′-pyridyl)tetrazolate] (**5a2**), bis[2-(2′,5′-difluorophenyl)-4-methoxypyridinato-*N*,$C^{2'}$]iridium(III) [5-(2′-pyridyl)tetrazolate] (**5a3**), bis[2-(3′,4′-difluorophenyl)-4-methoxypyridinato-*N*,$C^{2'}$]iridium(III) [5-(2′-pyridyl)tetrazolate] (**5a4**), and bis[2-(3′,5′-difluorophenyl)-4-methoxypyridinato-*N*,$C^{2'}$]iridium(III) [5-(2′-pyridyl)tetrazolate] (**5a5**). Interestingly, **5a4** exhibits 2′-coordinated and 6′-coordinated isomers. The coordination behavior of this ligand with iridium metal differed depending on the repulsion energy and the delocalization energy effects of the iridium complexes. X-ray structural analysis technique was successfully applied to interpret the different coordination behavior of **5a4**. In addition, introducing the methoxy group to the well-known ligand (2-difluorophenylpyridine) successfully expanded the band gap of iridium complexes and made **5a2** exhibit the bluest emission at 452 nm. To the best of our knowledge, this is one of the bluest OLEDs based on a 2-difluorophenylpyridine-iridium coordination emitter.

1. Introduction

The photophysical properties of bis- and tris-cyclometalated iridium(III) complexes have been investigated extensively.[1] The mixing of singlet and triplet excited states by doping phosphorescent dyes into a charge-transporting host as emissive layers greatly enhances the internal phosphorescence quantum efficiency of organic light-emitting diodes (OLEDs) toward 100%.[2] By adequate modification of the coordinated ligands, the emission color can be readily tuned from red/green to blue. However, blue phosphorescent emitters are more difficult to achieve than green and red emitters.[3]

To design efficient blue emitters, it is critical to understand the structure−photophysical property relationship. There are two strategies for achieving this purpose. The first is maintaining the LUMO energy and decreasing the HOMO energy. A famous class of blue phosphorescent emitters using 4′,6′-difluorophenylpyridine-based iridium complexes has been extensively studied,[2b,4] in which electron-withdrawing groups, fluoro atoms, are added in the phenyl ring, and the emission energy of the cyclometalated iridium complexes is expanded. The second method involves altering the LUMO energy by using *N*-pyrazolyl or *N*-heterocyclic carbene-based ligands. Both *fac*-Ir(flz)$_3$ and *fac*-Ir(pmi)$_3$ complexes display phosphorescence in the 480 nm and the near-UV region at room temperature, respectively.[3c] Moreover, these studies show that the photophysical properties of the cyclometalated iridium complexes can be finely tuned by systematic control of the nature and position of the substituents on the ligands.

Recently, Laskar et al. reported that the blue-emitting iridium(III) complex *fac*-Ir(F_2MeOppy)$_3$ exhibits emission color at 464 nm,[5] a property that is ascribed to the strong electron-donating substituents at the 4-position of the pyridyl moiety, raising the LUMO energy state of the iridium(III) complex. In this study, we apply this concept to introduce a methoxy substituent at the 4-position of pyridyl and systematic changes in the position of two fluoro substituents of the phenyl rings.[4c] Moreover, we applied the stronger electron-withrawing pyridyltetrazole as the third N^N chelating anion.[4d] On these bases, it is thus anticipated that the widest HOMO−LUMO gap can be achieved and can lead to a blue shift in emission.

2. Experimental Section

General Information and Materials. All starting materials were purchased from Aldrich and TCI and were used without further purification. Scheme 1 outlines how the ligand difluorophenylpyridine was synthesized and utilized for preparing a series of iridium complexes.[4c,6] 5-(2′-Pyridyl)tetrazole is a known compound and can

* Corresponding authors. (C.-H.Y.) Tel: +886-6-3847439. Fax: +886-6-3847289. E-mail: jasonyang0606@yahoo.com.tw. (I-W.S.) E-mail: iwsun@mail.ncku.edu.tw.

† Department of Chemistry, National Cheng Kung University.

‡ Nano-Powder & Thin Film Technology Center.

§ Department of Electrical Engineering, National Cheng Kung University.

(1) (a) King, K. A.; Spellane, P. J.; Watts, R. J. *J. Am. Chem. Soc.* **1985**, *107*, 1431. (b) Baldo, M. A.; Lamansky, S.; Burrows, P. E.; Thompson, M. E.; Forrest, S. R. *Appl. Phys. Lett.* **1999**, *75*, 4.

(2) (a) Lamansky, S.; Djurovich, P.; Murphy, D.; Abdel-Razzaq, F.; Lee, H.; Adachi, C.; Burrows, P. E.; Forrest, S. R. *J. Am. Chem. Soc.* **2001**, *123*, 4304. (b) Brooks, J.; Babayan, Y.; Lamansky, S.; Djurovich, P. I.; Tsyba, I.; Bau, R.; Thompson, M. E. *Inorg. Chem.* **2002**, *41*, 3055. (c) Wu, P. C.; Yu, J. K.; Song, Y. H.; Chi, Y.; Chou, P. T.; Peng, S. M.; Lee, G. H. *Organometallics* **2003**, *22*, 4938. (d) Tung, Y. L.; Wu, P. C.; Liu, C. S.; Chi, Y.; Yu, J. K.; Hu, Y. H.; Chou, P. T.; Peng, S. M.; Lee, G. H.; Tao, Y.; Carty, A. J.; Shu, C. F.; Wu, F. I. *Organometallics* **2004**, *23*, 3745.

(3) (a) Dedeian, K.; Shi, J.; Shepherd, N.; Forsythe, E.; Morton, D. C. *Inorg. Chem.* **2005**, *44*, 4445. (b) Yang, C. H.; Li, S. W.; Chi, Y. *Inorg. Chem.* **2005**, *44*, 7770. (c) Sajoto, T.; Djurovich, P. I.; Tamayo, A.; Yousufuddin, M.; Bau, R.; Thompson, M. E. *Inorg. Chem.* **2005**, *44*, 7992.

(4) Nonoyama, M. *Bull. Chem. Soc. Jpn.* **1974**, *47*, 767.

10.1021/om061101u CCC: $37.00
Publication on Web 03/06/2007

Scheme 1. Synthesis of Iridium Complexes

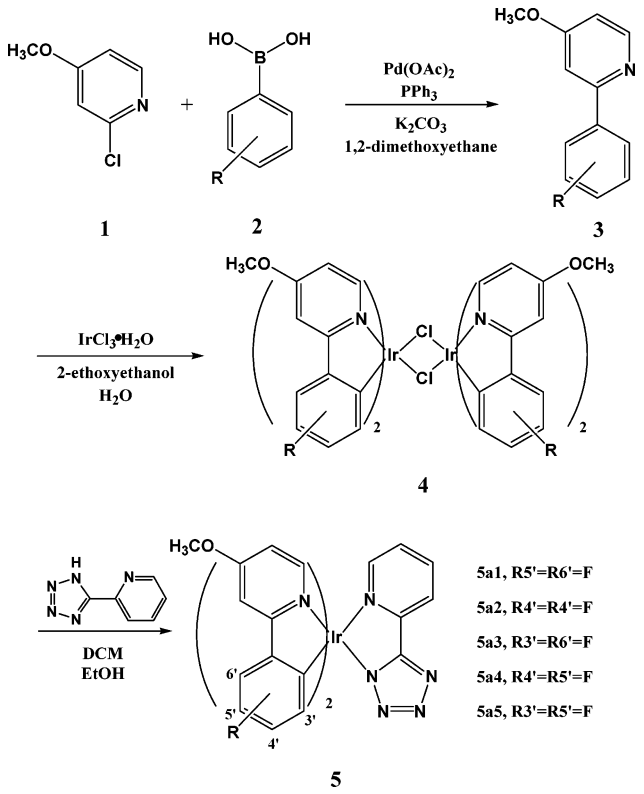

be prepared easily in one step from commercially available 2-cyanopyridine and sodium azide.[7] All synthetic procedures and manipulations involving $IrCl_3 \cdot H_2O$ and other Ir(III) species were carried out under a nitrogen atmosphere. ^1H NMR and ^{13}C NMR spectra were measured in CD_2Cl_2 solution on Bruker Avance-300 (300 MHz), AMX-400 (400 MHz), or Avance-500 (500 MHz) NMR spectrometers with tetramethylsilane (TMS) as the internal standard. The EI-MS were recorded on a Bruker APEX II. Melting points were measured using capillary melting point apparatus. HRMS spectra were obtained using a MAT-95XL high-resolution mass spectrometer. Elemental analyses have been carried out by using an Elementar vario EL III analyzer. The UV−vis spectra were measured in a 1×10^{-5} M CH_2Cl_2 solution on an Agilent 8453 spectrophotometer, and the photoluminescence spectra were recorded in a 1×10^{-5} M CH_2Cl_2 solution with a Hitachi model F-2500 fluorescence spectrophotometer.

Synthesis of 2-(2′,3′-Difluorophenyl)-4-methoxypyridine (3a1). 3a1 was prepared by a modified method (Scheme 1).[8] In a two-necked round-bottomed flask (25 mL) equipped with a reflux condenser 2,3-difluoroboronic (4.17 mmol, **2**) was added to a suspension of 2-chloro-4-methoxypyridine (3.79 mmol, **1**) in 1,2-dimethoxyethane (12 mL) at ambient temperature under nitrogen. After stirring for 5 min, triphenylphosphine (0.38 mmol), $Pd(OAc)_2$ (0.095 mmol), and potassium carbonate (7.1 mmol) were added to the suspension. The reaction mixture was heated to 80 °C (oil bath temperature) with rapid stirring. After cooling to ambient temperature, the mixture was extracted with ethyl acetate (3 × 15 mL), and the combined extracts were washed successively by brine and water and dried ($MgSO_4$). The oil phase was removed under reduced pressure and then purified by flash chromatography (*n*-hexane−ethylacetate = 4:1). The colorless liquid product was obtained in a 46% yield. EI-MS: *m*/*z* 221, $[M]^+$. ^1H NMR (acetone-d_6, 300 MHz): δ 8.45 (d, J = 5.7 Hz, 1H), 7.82−7.76 (m, 1H), 7.38−7.27 (m, 3H), 6.95 (dd, J = 5.7, 2.3 Hz, 1H), 3.81 (s, 3H). ^{13}C NMR (acetone-d_6, 75 MHz): δ 206.4, 167.0, 154.3, 153.4, 151.9, 130.5, 126.8, 125.2, 118.2, 111.5, 109.8, 55.8. Anal. Calcd for $C_{12}H_9F_2NO$: C, 65.20; H, 4.10; N, 6.33. Found: C, 65.11; H, 4.03; N, 6.37.

Synthesis of 2-(2′,4′-difluorophenyl)-4-methoxypyridine (3a2): colorless oil. Yield: 94%. EI-MS: *m*/*z* 221, $[M]^+$. ^1H NMR (acetone-d_6, 500 MHz): δ 8.82 (d, J = 5.7 Hz, 1H), 8.41−8.31 (m, 1H), 7.62 (t, J = 1.9 Hz, 1H), 7.55−7.53 (m, 2H), 7.22 (dd, J = 9.2, 2.5 Hz, 1H), 4.21 (2, 3H). ^{13}C NMR (acetone-d_6, 75 MHz): δ 206.2, 167.0, 163.0, 159.7, 154.4, 151.8, 133.4, 124.8, 112.3, 110.9, 104.9, 56.3. Anal. Calcd for $C_{12}H_9F_2NO$: C, 65.20; H, 4.10; N, 6.33. Found: C, 65.18; H, 4.07; N, 6.34.

Synthesis of 2-(2′,5′-difluorophenyl)-4-methoxypyridine (3a3): white needles. Yield: 70%. Mp: 93.2 °C. EI-MS: *m*/*z* 221, $[M]^+$. ^1H NMR (acetone-d_6, 300 MHz): δ 8.52 (d, J = 4.2 Hz, 1H), 7.78−7.77 (m, 1H), 7.31 (t, J = 1.4 Hz, 1H), 7.30−6.99 (m, 2H), 6.95 (dd, J = 4.2, 1.9 Hz, 1H), 3.98 (s, 3H). ^{13}C NMR (acetone-d_6, 75 MHz): δ 206.3, 167.1, 160.9, 158.5, 156.2, 153.9, 151.9, 118.8, 117.8, 111.5, 109.8, 55.9. Anal. Calcd for $C_{12}H_9F_2NO$: C, 65.20; H, 4.10; N, 6.33. Found: C, 65.07; H, 4.13; N, 6.24.

Synthesis of 2-(3′,4′-difluorophenyl)-4-methoxypyridine (3a4): white needles. Yield: 35%. Mp: 90.2 °C. EI-MS: *m*/*z* 221, $[M]^+$. ^1H NMR (acetone-d_6, 500 MHz): δ 8.81 (d, J = 5.8 Hz, 1H), 8.46−8.41 (m, 1H), 8.36−8.32 (m, 1H), 7.83 (d, J = 2.4 Hz, 1H), 7.95−7.75 (m, 1H), 7.25 (dt, J = 5.8, 2.4 Hz, 1H), 4.25 (s, 3H). ^{13}C NMR (acetone-d_6, 75 MHz): δ 206.4, 167.5, 157.4, 151.9, 133.4, 125.4, 118.1, 117.4, 111.9, 97.4, 56.7. Anal. Calcd for $C_{12}H_9F_2NO$: C, 65.20; H, 4.10; N, 6.33. Found: C, 65.14; H, 4.08; N, 6.24.

Synthesis of 2-(3′,5′-difluorophenyl)-4-methoxypyridine (3a5): white needles. Yield: 35%. Mp: 78.4 °C. EI-MS: *m*/*z* 221, $[M]^+$. ^1H NMR (acetone-d_6, 300 MHz): δ 8.51 (d, J = 5.6 Hz, 1H), 8.46−8.41 (m, 1H), 7.81 (dd, J = 9.3, 2.0 Hz, 2H), 7.55 (d, J = 2.3 Hz, 1H), 7.10−7.07 (m, 1H), 6.95 (dt, J = 5.6, 2.3 Hz, 1H), 4.00 (s, 3H). ^{13}C NMR (acetone-d_6, 75 MHz): δ 205.2, 166.8, 150.8, 109.5, 109.3, 106.5, 103.6, 98.8, 54.9. Anal. Calcd for $C_{12}H_9F_2NO$: C, 65.20; H, 4.10; N, 6.33. Found: C, 64.91; H, 4.15; N, 6.16.

Synthesis of bis[2-(2′,3′-difluorophenyl)-4-methoxypyridinato-*N*,*C*$^{2'}$]iridium(III) [5-(2′-pyridyl)tetrazolate] (5a1). The cyclometalated Ir(III) μ-chloro-bridged dimers (**4**) were synthesized by the method reported by Nonoyama.[6] 2-(2′,3′-Difluorophenyl)-4-methoxypyridine (**3a1**) (10.0 mmol) and 0.4 equiv of $IrCl_3 \cdot H_2O$ (Next Chimica) were heated in a 3:1 mixture of 2-ethoxyethanol and water. This slurry was heated at 100 °C for 24 h. After cooling to room temperature, the precipitate was filtered off and washed with deionized water. The solid obtained was placed in a flask and dispersed in dichloromethane and methanol. 5-(2′-Pyridyl)tetrazole was added to the solution, and the mixture was stirred at room temperature for 4−6 h. After drying in a vacuum, the crude product was washed with deionized water, followed by two portions of *n*-hexane and ether. The solid was dried, and column chromatography was used to give yellow, pure product **5a1** in 88.9% yield. FAB-MS: *m*/*z* 780, $[M + H]^+$. HRESI-MS: found *m*/*z* 780.1320, calcd for $C_{30}H_{21}F_4IrN_7O_2$ 780.1322. ^1H NMR (CD_2Cl_2, 300 MHz): δ 8.42 (d, J = 7.9 Hz, 1H), 8.02 (t, J = 7.9 Hz, 1H), 7.83−7.73 (m, 3H), 7.45 (d, J = 6.6 Hz, 1H), 7.35 (d, J = 6.5 Hz, 2H), 6.90−6.76 (m, 2H), 6.58−6.53 (m, 2H), 6.18−6.02 (m, 2H), 3.93 (s, 3H), 3.92 (s, 3H). ^{13}C NMR (CD_2Cl_2, 75 MHz): δ 157.5, 157.3, 140.9, 140.1, 139.6, 139.5, 138.5, 129.2, 116.6 (m, 2C), 116.0,

(5) (a) Adamovich, V.; Brooks, J.; Tamayo, A.; Alexander, A. M.; Djurovich, P. I.; D'Andrade, B. W.; Adachi, C.; Forrest, S. R.; Thompson, M. E. *New J. Chem.* **2002**, *26*, 1171. (b) Tamayo, A. B.; Alleyne, B. D.; Djurovich, P. I.; Lamansky, S.; Tsyba, I.; Ho, N. N.; Bau, R.; Thompson, M. E. *J. Am. Chem. Soc.* **2003**, *125*, 7377. (c) Coppo, P.; Plummer, E. A.; Cola, L. D. *Chem. Commun.* **2004**, 1774. (d) Yeh, S. J.; Wu, M. F.; Chen, C. T.; Song, Y. H.; Chi, Y.; Ho, M. H.; Hsu, S. F.; Chen, C. H. *Adv. Mater.* **2005**, *17*, 285.

(6) Laskar, I. R.; Hsu, S. F.; Chen, T. M. *Polyhedron* **2005**, *24*, 189.

(7) McManus, J. M.; Herbst, R. M. *J. Org. Chem.* **1959**, *24*, 1462.

(8) Yang, C. H.; Tai, C. C.; Huang, Y. T.; Sun, I. W. *Tetrahedron* **2005**, *61*, 4857.

Table 1. Crystallographic Data of 5a1, 5a2, 5a3, and 5a4

	5a1	5a2	5a3	5a4
formula	$C_{30}H_{20}F_4Ir_1N_7O_2$	$C_{30}H_{20}F_4Ir_1N_7O_2$	$C_{30}H_{20}F_4Ir_1N_7O_2$	$C_{30}H_{20}F_4Ir_1N_7O_2$
fw	778.73	778.73	778.73	778.73
space group	*C*2/*c*	*P*2(1)/*c*	$P\bar{1}$	*P*2(1)/*n*
a/Å	29.506(10)	8.8669(2)	8.6310(2)	13.0229(4)
b/Å	12.0480(2)	28.7378(5)	9.1750(2)	14.7972(4)
c/Å	22.2890(3)	11.2750(3)	17.8470(5)	14.2666(6)
α/Å	90.0000(10)	90.00	85.8330(10)	90.00
β/Å	128.3440(10)	103.3890(10)	78.0080(10)	100.6000(10)
γ/Å	90.0000(10)	90.00	82.8620(10)	90.00
V/Å^3	6214.38(13)	2794.95(11)	1370.14(6)	2702.29(16)
Z	8	4	2	4
no. of reflns measd	37 638	25 698	19 409	19 434
no. of indep reflns	5694 [$R_{(int)} = 0.1631$]	5233 [$R_{(int)} = 0.1231$]	5034 [$R_{(int)} = 0.0855$]	4936 [$R_{(int)} = 0.1045$]
no. of params	406	397	398	272
final R ($I > 2\sigma(I)$)	$R_1{}^a = 0.0490$, $wR_2{}^{b,c} = 0.1319$	$R_1{}^a = 0.0563$, $wR_2{}^{b,c} = 0.1215$	$R_1{}^a = 0.0458$, $wR_2{}^{b,c} = 0.1027$	$R_1{}^a = 0.0480$, $wR_2{}^{b,c} = 0.1192$
goodness of fit on F^2	1.140	1.069	1.099	1.004

^{a} $R_1 = \sum|F_o| - |F_c|/\sum|F_o|$. ^{b} $wR_2 = [\sum w[(F_o^2 - F_c^2)^2]/\sum[w(F_o^2)^2]]^{1/2}$. ^{c} $w = 1/\sigma^2(F_o^2) + (0.075P)^2]$, where $P = [\mathrm{Max}(F_o^2,0) + 2F_c^2]/3$.

Table 2. Selected Bond Lengths [Å] and Angles [deg] for 5a1, 5a2, 5a3, and 5a4

		5a1	
Ir1−N1	2.060(5)	Ir1−N2	2.045(5)
Ir1−N3	2.121(6)	Ir1−N7	2.173(5)
Ir1−C12	1.999(7)	Ir1−C13	2.005(6)
C18−C19	1.463(8)	C6−C7	1.468(8)
C25−C26	1.481(8)		
N3−Ir1−N7	75.96(2)	C12−Ir1−N1	80.3(2)
C13−Ir1−N2	80.3(2)	N1−Ir1−N3	94.32(2)
C12−Ir1−N2	97.3(2)	C12−Ir1−N7	96.3(2)
		5a2	
Ir1−C24	2.002(1)	Ir1−C12	2.005(8)
Ir1−N1	2.051(7)	Ir1−N2	2.052(7)
Ir1−N3	2.128(6)	Ir1−N7	2.174(8)
C18−C19	1.467(1)	C6−C7	1.472(1)
C25−C26	1.466(1)		
N3−Ir1−N7	75.9(3)	C12−Ir1−N1	80.9(3)
C24−Ir1−N2	80.9(3)	N2−Ir1−N3	89.6(3)
N1−Ir1−N3	94.8(3)	C12−Ir1−N7	97.0(3)
		5a3	
Ir1−N1	2.096(7)	Ir1−N5	2.154(7)
Ir1−N6	2.041(7)	Ir1−C18	2.023(8)
Ir1−C30	2.029(8)	Ir1−N7	2.049(6)
C12−C13	1.480(1)	C24−C25	1.466(12)
C1−C2	1.459(1)		
N1−Ir1−N5	76.5(3)	N7−Ir1−N1	84.2(3)
C18−Ir1−N6	80.3(3)	C30−Ir1−N7	80.2(3)
N7−Ir1−N5	96.6(3)	C18−Ir1−N5	97.8(3)
		5a4	
Ir1−C12	2.026(9)	Ir1−N2	2.064(7)
Ir1−N3	2.114(7)	Ir1−N7	2.181(7)
Ir1−C13	2.018(9)	Ir1−N1	2.038(8)
C18−C19	1.463(1)	C6−C7	1.471(1)
C25−C26	1.454(1)		
C13−Ir1−N2	80.1(3)	N3−Ir1−N7	76.2(3)
C12−Ir1−N1	80.4(3)	N1−Ir1−N3	93.7(3)
C13−Ir1−N1	94.5(4)	C12−Ir1−N2	96.4(3)

112.9, 108.2 (m, 2C), 100.1 (m, 2C), 46.2, 46.1. $^{19}F\{^1H\}$ NMR (CD_2Cl_2, 282 MHz): δ −141.68 (d, J = 19.4 Hz, 1F), −142.06 (d, J = 16.9 Hz, 1F), −148.98 (d, J = 16.9 Hz, 1F), −149.81 (m, 1F). Anal. Calcd for $C_{30}H_{20}F_4IrN_7O_2 \cdot 1/2CH_2Cl_2$: C, 44.60; H, 2.56; N, 11.94. Found: C, 44.36; H, 2.95; N, 11.76.

Synthesis of bis[2-(2′,4′-difluorophenyl)-4-methoxypyridinato-*N*,*C*$^{2'}$]iridium(III) [5-(2′-pyridyl)tetrazolate] (5a2): pale yellow solid. Yield: 62.4%. FAB-MS: *m*/*z* 780, $[M + H]^+$. HRESI-MS: found *m*/*z* 780.1321, calcd for $C_{30}H_{21}F_4IrN_7O_2$ 780.1322. ^1H NMR (CD_2Cl_2, 300 MHz): δ 8.39 (d, J = 7.9 Hz, 1H), 7.99−7.97 (m, 1H), 7.82 (d, J = 5.1 Hz, 1H), 7.79 (t, J = 3.1 Hz, 1H), 7.75 (t, J = 2.9 Hz, 1H), 7.34−7.21 (m, 3H), 6.55−6.47 (m, 4H), 5.98 (dd, J = 8.6, 2.2 Hz, 1H), 5.81 (dd, J = 8.7, 2.2 Hz, 1H), 3.91 (s, 3H), 3.90 (s, 3H). ^{13}C NMR (CD_2Cl_2, 75 MHz): δ 157.6, 157.4, 140.6, 140.1, 139.5, 139.2, 129.4, 116.2, 112.9, 104.3 (m, 2C), 99.5 (m, 2C), 88.0 (m, 2C), 46.2, 46.1. $^{19}F\{^1H\}$ NMR (CD_2Cl_2, 282 MHz): δ −111.93 (t, J = 8.5 Hz, 1F), −112.50 (dd, J = 14.1, 11.3 Hz, 1F), −113.99 (t, J = 11.3 Hz, 1F), −114.59 (t, J = 11.3 Hz, 1F). Anal. Calcd for $C_{30}H_{20}F_4IrN_7O_2 \cdot CH_2Cl_2$: C, 43.11; H, 2.55; N, 11.36. Found: C, 43.56; H, 2.87; N, 11.18.

Synthesis of bis[2-(2′,5′-difluorophenyl)-4-methoxypyridinato-*N*,*C*$^{2'}$]iridium(III) [5-(2′-pyridyl)tetrazolate] (5a3): pale yellow solid. Yield: 84.0%. FAB-MS: *m*/*z* 780, $[M + H]^+$. HRESI-MS: found *m*/*z* 780.1322, calcd for $C_{30}H_{21}F_4IrN_7O_2$ 780.1322. ^1H NMR (CD_2Cl_2, 500 MHz): δ 8.32 (d, J = 7.8 Hz, 1H), 7.90 (td, J = 7.8, 1.5 Hz, 1H), 7.80 (d, J = 5.2 Hz, 1H), 7.75−7.65 (m, 2H), 7.23−7.19 (m, 3H), 6.71−6.69 (m, 2H), 6.52−6.38 (m, 2H), 6.35−6.29 (m, 2H), 3.81 (s, 3H), 3.80 (s, 3H). ^{13}C NMR (CD_2Cl_2, 75 MHz): δ 157.2, 156.6, 153.5, 149.4, 141.2, 140.0, 139.7, 139.5, 129.6, 126.5, 118.8, 116.4, 113.1, 107.0 (m, 2C), 100.5 (m, 2C), 99.3 (m, 2C), 46.0. $^{19}F\{^1H\}$ NMR (CD_2Cl_2, 282 MHz): δ −114.10 (d, J = 22.6 Hz, 1F), −115.12 (d, J = 22.6 Hz, 1F), −123.19 (s, 1F), −123.67 (s, 1F). Anal. Calcd for $C_{30}H_{20}F_4IrN_7O_2 \cdot 1/2CH_2Cl_2$: C, 44.60; H, 2.56; N, 11.94. Found: C, 44.45; H, 2.82; N, 11.84.

Synthesis of bis[2-(3′,4′-difluorophenyl)-4-methoxypyridinato-*N*,*C*$^{2'}$]iridium(III) [5-(2′-pyridyl)tetrazolate] (5a4): yellow solid. Yield: 85.0%. FAB-MS: *m*/*z* 780, $[M + H]^+$. HRESI-MS: found *m*/*z* 780.1324, calcd for $C_{30}H_{21}F_4IrN_7O_2$ 780.1322. Anal. Calcd for $C_{30}H_{20}F_4IrN_7O_2 \cdot 1/2CH_2Cl_2$: C, 44.60; H, 2.56; N, 11.94. Found: C, 44.60; H, 2.75; N, 12.02.

Synthesis of Bis[2-(3′,5′-difluorophenyl)-4-methoxypyridinato-*N*,*C*$^{2'}$]iridium(III) [5-(2′-pyridyl)tetrazolate] (5a5): yellow solid. Yield: 94.0%. FAB-MS: *m*/*z* 780, $[M + H]^+$. HRESI-MS: found *m*/*z* 780.1322, calcd for $C_{30}H_{21}F_4IrN_7O_2$ 780.1322. ^1H NMR (CD_2Cl_2, 300 MHz): δ 8.45 (d, J = 7.7 Hz, 1H), 8.00−7.97 (m, 1H), 7.90 (d, J = 5.2 Hz, 1H), 7.38−7.13 (m, 7H), 6.48−6.39 (m, 4H), 3.90 (s, 3H), 3.89 (s, 3H). ^{13}C NMR (CD_2Cl_2, 75 MHz): δ 174.1, 166.9, 166.8, 151.1, 149.8, 149.6, 149.4, 139.1, 125.9, 122.7, 109.3 (m, 2C), 107.5 (m, 2C), 104.8 (m, 2C), 55.8, 55.7. $^{19}F\{^1H\}$ NMR(CD_2Cl_2, 282 MHz): δ −101.48 (s, 1F), −103.02 (s, 1F), −119.49 (s, 1F), −120.75 (s, 1F). Anal. Calcd for $C_{30}H_{20}F_4IrN_7O_2 \cdot 1/2CH_2Cl_2$: C, 44.59; H, 2.61; N, 11.92. Found: C, 44.60; H, 2.65; N, 12.05.

X-ray Structural Analysis. Crystals of **5a1**, **5a2**, **5a3**, and **5a4** were obtained from solutions of CH_2Cl_2−*n*-hexane. The crystal data were selected for indexing and intensity data collection on a Siemens SMART CCD diffractometer equipped with a normal focus, 3 kW sealed tube X-ray source at 200 K. No significant decay was observed for all samples during the data collection. Data were processed on a PC using the Bruker AXS SHELXTL NT software package. Neutral atom scattering factors were taken from

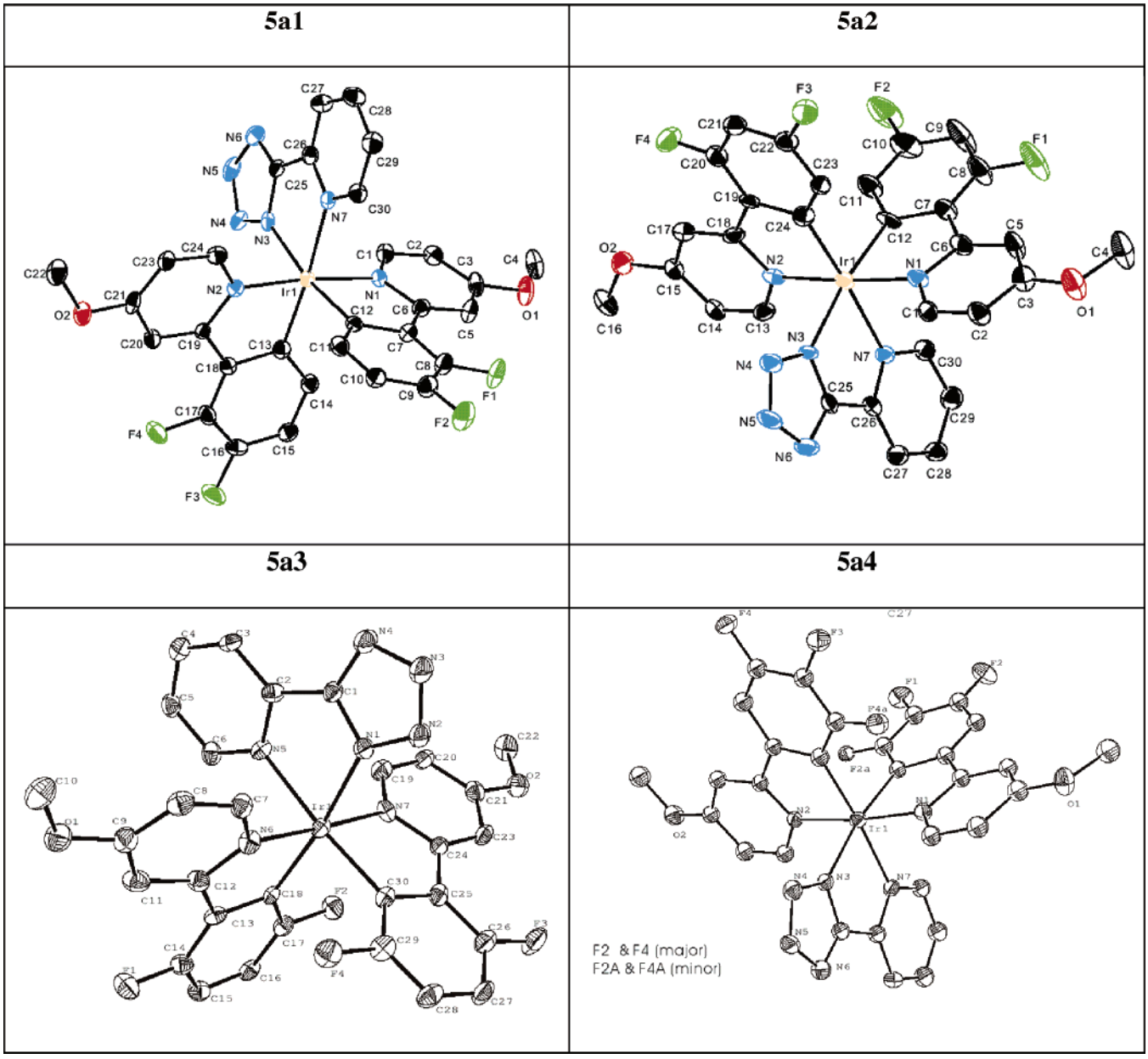

Figure 1. ORTEP diagram of **5a1**, **5a2**, **5a3**, and **5a4**.

Cromer and Waber. The crystals of **5a1**, **5a2**, and **5a4** belong to the monoclinic space group *C*2/*c*, *P*21/*c*, and *P*21/*n*, respectively. The crystal of **5a3** belongs to the triclinic space group *P*1. All structures were solved by direct methods. All non-hydrogen atoms were refined anisotropically. The positions for all hydrogen atoms were either calculated or located directly from different Fourier maps, and their contributions to the structural factor calculation were included. The crystallographic data of **5a1**, **5a2**, **5a3**, and **5a4** are given in Table 1, and selected bond lengths and angles are summarized in Table 2.

Crystallographic data (excluding structure factors) for **5a1**, **5a2**, **5a3**, and **5a4** have been deposited with the Cambridge Crystallographic Data Centre as supplementary publication numbers CCDC 294684, 608610, 601713, and 601714, respectively. Copies of the data can be obtained, free of charge, on application to CCDC, 12 Union Road, Cambridge CB2 1EZ, UK [fax: 144-(0)1223-336033 or e-mail: deposit@ccdc.cam.ac.uk].

Electrochemistry. Cyclic voltammograms (CV) were performed with a voltammetric analyzer (Bioanalytical Model CV-50W). All CV measurements were carried out in CH_2Cl_2 containing 0.1 M tetrabutylammonium perchlorate (n-Bu_4NClO_4) as the supporting electrolyte. A Pt disk electrode was used as the working electrode, a Pt wire as the counter electrode, and a $Ag/AgNO_3$ as the reference electrode. The ferrocenium/ferrocene redox couple in CH_2Cl_2/n-Bu_4NClO_4 occurs at $E^{o\prime} = +0.35$ V versus $Ag/AgNO_3$. The oxidation potential of the Ir complexes is reported versus the ferrocenium/ferrocene redox couple.

OLEDs Fabrication and Measurement. Pre-patterned ITO glasses with an effective device of 0.16 cm^2 were cleaned in detergent for 10 min and then washed with a large amount of doubly distilled water. After being sonicated in pure water for 5 min, these glasses were dried in an oven at 180 °C for 90 min. The organic layers were deposited thermally at a rate of 0.1 nm/s and pressure of $\sim 1 \times 10^{-6}$ Torr in a deposition system. Aluminum was deposited as a cathode. Electroluminescence data were measured with a SpectraScan PR650.

3. Results and Discussion

Synthesis and Characterization. Scheme 1 shows the synthesis of the ligands and the iridium complexes. After Suzuki coupling of 4-methoxy-2-chloropyridine (**1**) and difluorophen-

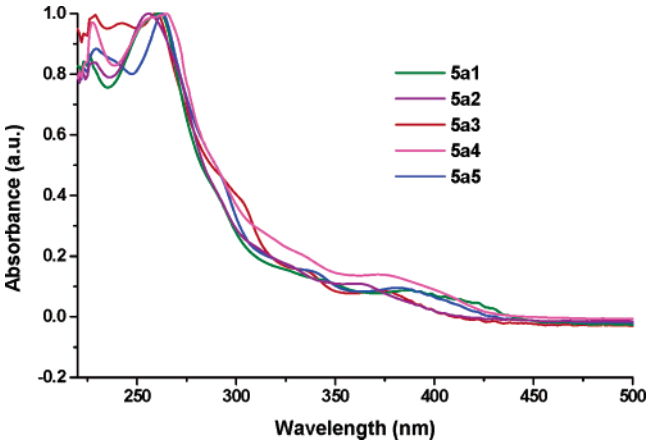

Figure 2. Normalized UV−vis spectra of iridium complexes in CH_2Cl_2 (10^{-5} M).

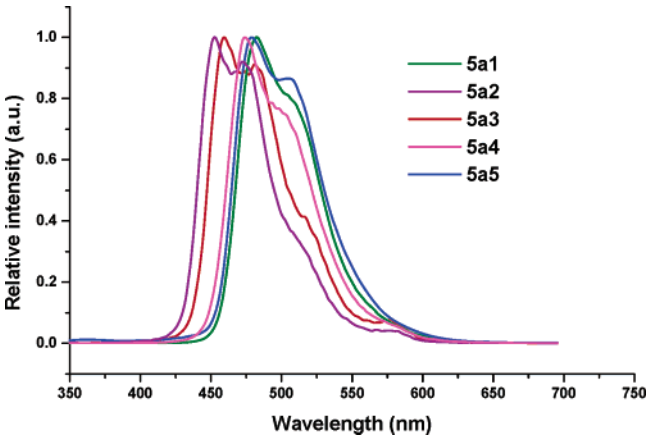

Figure 3. Normalized photoluminescence spectra of iridium complexes in CH_2Cl_2.

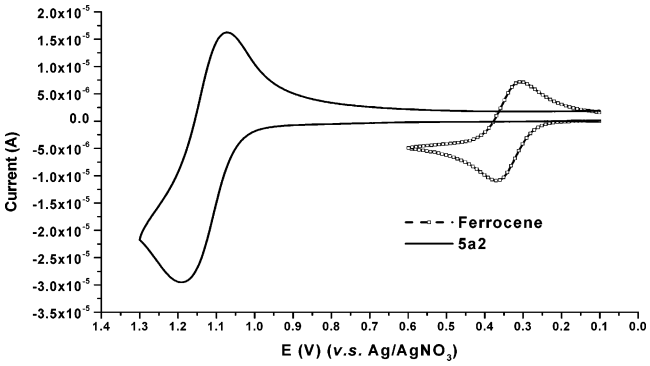

Figure 4. Cyclic voltammogram of the iridium(III) complex **5a1**. CV data were measured in CH_2Cl_2 solution with Pt disk electrode, $Ag/AgNO_3$ electrode, and Pt electrode as working, reference, and counter electrodes, respectively. The scan rate was 100 mV/s, and ferrocene was used as a reference.

ylboronic acid (**2**), a series of analogous ligands including 2-(2′,3′-difluorophenyl)-4-methoxypyridine (**3a1**), 2-(2′,4′-difluorophenyl)-4-methoxypyridine (**3a2**), 2-(2′,5′-difluorophenyl)-4-methoxypyridine (**3a3**), 2-(3′,4′-difluorophenyl)-4-methoxypyridine (**3a4**), and 2-(3′,5′-difluorophenyl)-4-methoxypyridine (**3a5**) were obtained and characterized. The desired iridium complexes **5aX** (**X** = 1, 2, 3, 4, 5) were synthesized from the above ligands and 5-(2′-pyridyl)tetrazole and characterized by ^{1}H NMR, ^{13}C NMR, mass spectrometry, and elemental analyses.

In the synthesis of the iridium(III) complex, it was found that **5a4** exhibits the 2′-coordinated and the 6′-coordinated isomers, and their ^{1}H NMR and ^{13}C NMR spectra are very difficult to resolve. After X-ray structural analysis, we found bis[2-(4′,5′-difluorophenyl)-4-methoxypyridinato-*N*,$C^{2'}$]iridium(III) [5-(2′-pyridyl)tetrazolate] (exo-form) is the major product and bis[2-(3′,4′-difluorophenyl)-4-methoxypyridinato-*N*,$C^{2'}$]-iridium(III) [5-(2′-pyridyl)tetrazolate] (endo-form) is the minor. This result probably originates from the balancing between the electron repulsion energy and delocalization energy.[9]

Table 3. Photophysical Properties of Iridium Complexes

complex	absorbance[a] λ (nm) (log ϵ)[b]	emission λ_{max} (nm)[a]	$\Phi_{degassed}$[c]
5a1	261(5.52), 388(4.47)	482	1.90
5a2	256(5.72), 361(4.76)	452, 473	0.22
5a3	259(5.56), 372(4.49)	459, 481	0.23
5a4	265(5.54), 372(4.69)	474, 498	0.63
5a5	263(5.69), 382(4.67)	479, 505	1.89

[a] All data were obtained in CH_2Cl_2 solution (concentration = 10^{-5} M). [b]The unit of ϵ is M^{-1} cm^{-1}. [c]The quantum yields (Φ) in degassed CH_2Cl_2 solution were measured at 298 K and used $FIrN_4$ (Φ = 1) as a standard.

Single crystals of **5a1**−**5a4** were obtained from CH_2Cl_2−*n*-hexane solutions. The crystal structure determined by X-ray diffraction analysis is shown in Figure 1. The corresponding crystallographic data and selected bond lengths and angles are summarized in Tables 1 and 2. Despite the similarity of the structure of these four complexes, they crystallized in different space groups. Complexes **5a1**, **5a2**, **5a3**, and **5a4** belong to the monoclinic space group *C*2/*c*, the monoclinic space group *P*21/*c*, the triclinic space group *P*1, and the monoclinic space group $P2_1/n$, respectively. The diversity of space groups of this series of complexes suggests that the packing of these complexes is very sensitive to the different position of substituents of the ligands. The molecular structures of the complexes are very similar to each other. As depicted in Figure 1, these four complexes reveal a distorted octahedral geometry around iridium, consisting of two cyclometalated difluorophenyl-4-methoxypyridine ligands and one pyridyltetrazole ligand. Because the three ligands split the d-orbitals of the central metal, iridium, unequally, the crystal structures of these complexes are distorted octahedrons and prefer the cis-C−C, trans-N−N chelate disposition.

As depicted in Figure 1, the C−C and C−N bond lengths and angles observed in these four complexes are typical for aromatic molecules. The bond length of Ir−N in the complexes is found to be longer than the Ir−C bond length. Interestingly, due to steric effects, the Ir−C bond length of **5a3** ($Ir-C_{av}$ = 2.026(8) Å) is longer than that in **5a1** ($Ir-C_{av}$ = 2.002(7) Å) and **5a2** ($Ir-C_{av}$ = 2.003(1) Å). Due to steric interactions, the difluorophenyl groups are not coplanar with the methoxypyridine group. X-ray data show that the dihedral angle between the two planes of complexes is always smaller than 5°. This is different from the data of red iridium complexes.[10] We speculate that the π electron density of difluorophenyl and methoxypyridine is smaller than in the phenyl and isoquinoline ring and the fluoro-substituted groups contribute less to the steric effect. This prevents the twist of the difluorophenyl and methoxypyridine rings not seen. Summaries of the refinement details, resulting factors, bond lengths, and bond angles are given in Tables 1 and 2.

Photophysical Data. The absorption and photoluminescence spectra of iridium complexes in CH_2Cl_2 solutions are depicted

(9) Yang, C. H.; Su, W. L.; Fang, K. U.; Wang, S. P.; Sun, I. W. *Organometallics* **2006**, *25*, 4514.

(10) (a) Huang, Y. T.; Chuang, T. H.; Shu, Y. L.; Kuo, Y. C.; Wu, P. L.; Yang, C. H.; Sun, I. W. *Organometallics* **2005**, *24*, 6230. (b) Hwang, F. M.; Chen, H. Y.; Chen, P. S.; Liu, C. S.; Chi, Y.; Shu, C. F.; Wu, F. L.; Chou, P. T.; Peng, S. M.; Lee, G. H. *Inorg. Chem.* **2005**, *44*, 1344. (c) Fang, K. H.; Wu, L. L.; Huang, Y. T.; Yang, C. H.; Sun, I. W. *Inorg. Chim. Acta* **2006**, *359*, 441.

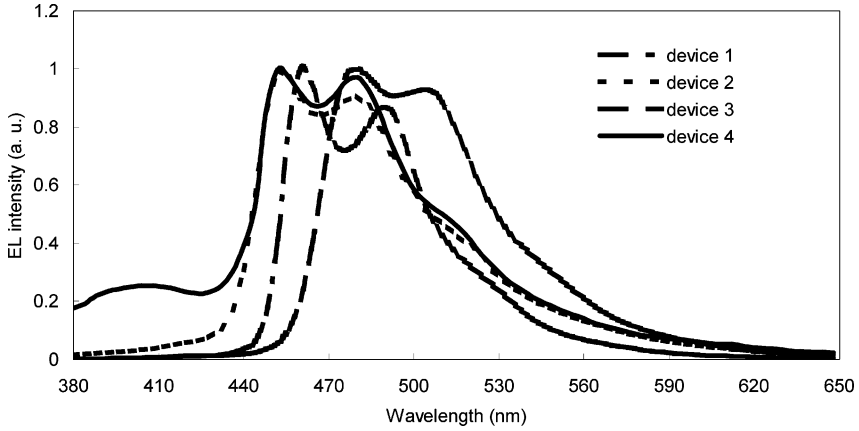

Figure 5. Electroluminescence spectra of devices 1 (TCB:FIrN4), 2 (TCB:**5a2**), 3 (TCB:**5a5**), and 4 (CBP:**5a2**) at 8 V.

Table 4. Electrochemical Data, HOMO, LUMO, and Energy Gap of the Iridium(III) Complexes

complex	$E^a_{p(ox)}$ (mV)	$E^c_{p(ox)}$ (mV)	$E_{1/2(ox)}$ (mV)[a]	HOMO (eV)[c]	LUMO (eV)[d]	energy gap (eV)
5a1	1190	1070	1130 [790][b]	−5.59	−2.77	2.82
5a2	1340	1260	1300 [960][b]	−5.76	−2.76	3.00
5a3	1314	1244	1279 [939][b]	−5.74	−2.71	3.03
5a4	1136	1012	1074 [734][b]	−5.54	−2.74	2.80
5a5	1217	1145	1181 [841][b]	−5.64	−2.76	2.88

[a] $E_{1/2(ox)} = 1/2(E^a_p + E^c_p)$ (vs Ag^+/Ag). [b] $E_{1/2(ox)}$ vs ferrocene/ferrocenium. [c] Data were collected in CH_2Cl_2 solution containing 0.001 M iridium complexes by cyclic voltammograms. [d] Data were collected in CH_2Cl_2 solution by a UV−vis spectrophotometer.

Table 5. Electroluminescence Data for Iridium(III) Complexes

	$FIrN_4$ (device 1)	**5a2** (device 2)	**5a5** (device 3)
luminance (cd/m^2)	12.2[a]	10.2[a]	13.2[a]
	269.3[b]	111.8[b]	236.8[b]
	1012.0[c]	417.7[c]	1046.0[c]
	1861.0[d]	799.8[d]	
luminous efficiency (cd/A)	7.19[a]	1.91[a]	18.51[a]
	6.70[b]	1.13[b]	11.29[b]
	4.47[c]	0.81[c]	8.05[c]
	2.47[d]	0.49[d]	
power efficiency (lm/W)	3.77[a]	1.00[a]	9.69[a]
	2.63[b]	0.44[b]	4.43[b]
	1.41[c]	0.26[c]	2.53[c]
	0.65[d]	0.13[d]	
current density (mA/cm^2)	0.17[a]	0.53[a]	0.07[a]
	4.02[b]	9.87[b]	2.10[b]
	22.62[c]	51.42[c]	13.00[c]
	75.38[d]	164.65[d]	
CIE	$x = 0.16$	$x = 0.18$	$x = 0.22$
	$y = 0.26$	$y = 0.23$	$y = 0.45$

[a] For each parameter, the data in different rows correspond to those measured at different voltages: in this case, 6 V. [b] 8 V. [c] 10 V. [d] 12 V.

in Figures 2 and 3. The data of all the iridium complexes are summarized in Table 3. The strong absorption bands in the ultraviolet region at about 250−280 nm with distinct vibronic features are assigned to the spin-allowed intraligand $^1\pi-\pi^*$ transitions. The next lower energy in the shoulder region of $^1\pi-\pi^*$ transitions at about 280−350 nm can be ascribed to the typical spin-allowed metal to ligand charge-transfer (^{1}MLCT) transition, while their extinction coefficients at peak wavelengths are in the range 4500−5200 M^{-1} cm^{-1}.[4,11] The weak shoulders extending into the visible region at 350−420 nm are believed to be associated with both spin−orbit coupling enhanced $^3\pi-\pi^*$ and ^{3}MLCT (spin-forbidden metal to ligand charge-transfer) transitions, and their extinction coefficients at peak wavelengths are in the range 4200−4800 M^{-1} cm^{-1}.

Highly intensive luminescence was observed for the iridium complexes in CH_2Cl_2 with λ_{max} at 452−479 nm. In comparison to $FIrN_4$ (iridium(III) bis(4,6-difluorophenylpyridinato)(5-(pyridine-2-yl)-1*H*-tetrazolate, λ_{max} at 461 nm),[4d] **5a2** shows a ∼9 nm hypsochromic shift in the photoluminescence peak. This blue shift effect can also be observed in the MLCT transition (as shown in Figure 2 and Table 3). As expected, the electron-donating methoxy group was incorporated onto the pyridyl ring to raise the LUMO energy and thereby successfully increased the energy gap of the emitting excited state. On the other hand, **5a1**, **5a4**, and **5a5** show a ∼13−21 nm bathochromic shift in comparison with $FIrN_4$. We suspect that a large amount of the electron density at the HOMO is centered at the 5′-position of the phenyl ring,[2b] and the weak π donation from the 5′-fluoro group raises the HOMO level, resulting in the red shift in the emission spectrum.

Redox Chemistry. Cyclic voltammetry was conducted on a Pt disk electrode (BAS Co.) in CH_2Cl_2 solutions containing 0.001 M of the iridium complexes and 0.1 M tetra-*n*-butylammonium perchlorate as the supporting electrolyte. A typical voltammogram of the iridium complex **5a1** is shown in Figure 4 together with the voltammogram of ferrocene. The electrochemical data of all the compounds are collected in Table 4. It shows that all the iridium complexes undergo a quasi-reversible oxidation because of the instability of the oxidative intermediates, and no reduction process was observed within the solvent cathodic potential limit.[4b,10a] The energy level of the LUMO was evaluated from the long-wavelength absorption edge using the theory reported by Burrows et al.[12] The $E_{1/2}$ data of the iridium complex

(11) Laskar, I. R.; Chen, T. M. *Chem. Mater.* **2004**, *16*, 111.

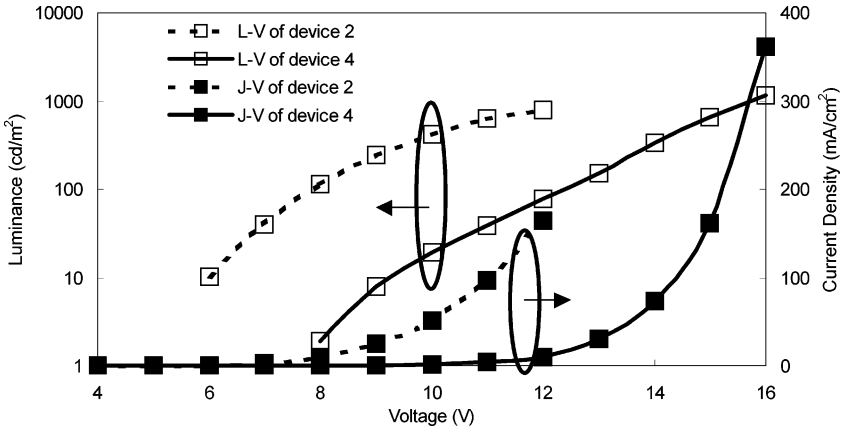

Figure 6. Luminance and current density as a function of applied voltage for devices 2 and 4.

$FIrN_4$ exhibit a higher value (1382 mV) than others (1074−1300 mV). This fact implies that after introducing an electron-donating group (methoxy group) to the pyridyl ring the iridium complexes are oxidized more easily. The summarized $E_{1/2}$, HOMO, LUMO, and energy gap data of the complexes **5a2** and **5a3**, shown in Table 4, are very close to each other. The $E_{1/2}$ of complexes **5a1**, **5a4**, and **5a5** show more negative potential (1130, 1074, and 1181 mV, respectively) in comparison to **5a2** and **5a3** (1300 and 1279 mV). The HOMO and energy gap values of the iridium complexes show the same tendency in comparison to photoluminescent and electroluminescent data. This result agrees with speculation that the electron density of the HOMO is centered at the 5′-position of the phenyl ring.

Device Properties. Using the phosphors discussed above, it is possible to prepare blue-light-emitting OLEDs. For the iridium(III)-based devices, we have fabricated **FIrN4**, **5a2**, and **5a5** as dopants into the emissive layer of OLEDs. Devices were fabricated by high-vacuum (10^{-6} Torr) thermal evaporation on precleaned indium−tin oxide (ITO) glass substrates. The device structures were ITO/2-TNATA (40 nm)/NPB (20 nm)/TCB: 6% dopant (30 nm)/BCP (10 nm)/Alq_3 (30 nm)/LiF (1 nm)/Al (100 nm). Figure 5 shows the normalized EL spectra of OLEDs with different dopant materials in TCB (device 1−3) and **5a2** in CBP (device 4). Compared to the EL spectra of devices 1−3 as shown in Figure 5, device 2 has the bluest light emission with a peak at 454 nm and a shoulder at 480 nm. The $CIE_{x,y}$ coordinates of device 2 were calculated to be 0.18 and 0.23. To the best of our knowledge, this is one of the bluest OLEDs based on an organic phosphorescent emitter. Similar to the PL spectra in solution, the extent of spectral shifting of the emission wavelength remained the same for EL spectra of device 2 (λ_{max} = 454 nm) and device 3 (λ_{max} = 482 nm). The optoelectrical characteristics of these devices are listed in Table 5. For device 2, a turn-on voltage of 6 V, maximum luminance of 800 cd/m^2 at 12 V, power efficiency of 1.00 lm/W, and current efficiency of 1.91 cd/A at 6 V were achieved. Moreover, the power efficiency and current efficiency at 100 cd/m^2 are 0.44 lm/W and 1.13 cd/A, respectively. Compared to devices 1 and 3, device 2 shows poor device efficiency, and this can be attributed to the molecular aggregation upon operation, which leads to the poor efficiency of OLEDs.

To compare with a CBP host, device 4 with a configuration of ITO/NPB (20 nm)/CBP: **5a2** (30 nm, 6%)/BCP (10 nm)/Alq_3 (30 nm)/LiF (1 nm)/Al (100 nm) was fabricated under the same conditions. It is worth pointing out that the hole-injection layer of 2-TNATA was not used in device 4. The current−voltage and voltage−luminescence characteristics of devices 2 and 4 are presented in Figure 6. For device 4, a turn-on voltage of 8 V, maximum luminance of 1140 cd/m^2 at 16 V, power efficiency of 0.45 lm/W, and current efficiency of 1.31 cd/A at 9 V were achieved. At 100 cd/m^2, the power efficiency and current efficiency are 0.12 lm/W and 0.50 cd/A, respectively. It is noted that although the maximum brightness decreased from 1140 to 800 cd/m^2, the maximum efficiency increased from 0.45 to 1.00 lm/W and the turn-on voltage decreased from 8 to 6 V in device 2. The lower turn-on voltage of device 2 can be attributed to the excellent hole-injecting property of 2-TNATA.[13] The improved efficiency of device 2 may be explained in terms of the higher triplet energies of TCB used in the devices.[14] From the EL spectra, as shown in Figure 5, there exists additional emission centering at around 410 nm when replacing TCB as a host to CBP. The additional emission was attributed to the CBP host. From this observation, we speculate that there was a very efficient energy transfer from the TCB triplet states to the **5a2** triple states and excellent triplet energy confinement on the **5a2** molecules, leading to high external quantum efficiency.[14]

4. Conclusion

Blue-emitting Ir(III) complexes based on the difluorophenyl-4-methoxypyridine and 5-(2′-pyridyl)tetrazole ligands were synthesized. The emission characteristics of these complexes are governed by the electron density of the cyclometalating ligand. The different substituted position of the fluoro atoms in the phenyl ring and methoxy group in the pyridine ring expand the band gap of iridium complexes, and an extremely blue emission at 452 nm was achieved for **5a2**. Further optimization of device efficiencies is still in progress. This work would facilitate the designing of new ligands for blue-light-emitting iridium complexes.

Acknowledgment. This work was supported by the National Science Council of the Republic of China, Taiwan.

Supporting Information Available: X-ray crystallographic data, including cif files for **5a1**, **5a2**, **5a3**, and **5a4**, are available free of charge via the Internet at http://pubs.acs.org.

OM061101U

(12) Burrows, P. E.; Shen, Z.; Bulovic, V.; McCarty, D. M.; Forrest, S. R. *J. Appl. Phys.* **1996**, *79*, 7991.

(13) Shirota, Y.; Kuwabara, Y.; Okuda, D.; Okuda, R.; Ogawa, H.; Inada, H.; Wakimoto, T.; Nakada, H.; Yonemoto, Y.; Kawami, S.; Imai, K. *J. Lumin.* **1997**, *985*, 72.

(14) Tokito, S.; lijima, T.; Suzuri, Y.; Kita, H.; Tsuzuki, T.; Sato, F. *Appl. Phys. Lett.* **2003**, *83*, 569.